On the application of horizontal ADCPs to suspended sediment transport surveys in rivers

S. A. Moore, Jérôme Le Coz, David Hurther

Author-produced version of the article published in Continental Shelf Research (2012), vol.46, p. 50-63
The original publication is available at http://www.sciencedirect.com/ doi : 10.1016/j.csr.2011.10.013

On the Application of Horizontal ADCPs to Suspended Sediment Transport Surveys in Rivers

S. A. Moore [a,*], J. Le Coz [a], D. Hurther [b], A. Paquier [a]

[a] *Cemagref UR HHLY, Hydrology Hydraulics,*

3 bis quai Chauveau, CP 220, 69336 Lyon, Cedex 09, France

[b] *Laboratoire des Ecoulements Géophysiques et Industriels, Domaine Universitaire,*

BP 53, 38041 Grenoble, Cedex 09, France

Abstract

In the last five years, horizontal Acoustic Doppler Current Profilers have come onto the market as an instrument designed to measure real-time horizontal current profiles from a permanent fixed mount. The focus of this paper is on the feasibility of using these commercial instruments to measure suspended sediment fluxes in rivers. Measurements are presented from a study site that was equipped with an optical turbidity meter and three horizontal ADCPs operating at 300 kHz, 600 kHz and 1200 kHz between November 2009 and June 2010. Laser grain size measurements showed the primary particles of the suspended sediment to be predominantly silts with some clay and occasionally some fine sand. Measurements of sediment attenuation by the three horizontal ADCPs are presented for two high concentration events during which concentrations reached 2.5 and 8 kg/m^3, respectively. Very clear linear relationships are seen between sediment attenuation and particle concentration and the sediment attenuation is consistent with the theory for viscous absorption by

fine sediments. Using the relationship between attenuation and concentration, we are able to reconstruct the concentration time series for events during which the turbidity data are unavailable. Our findings show that, when properly positioned, horizontal ADCPs can provide suitable measurements of sediment transport during extreme river flow conditions such as floods, at least for predominantly silt-sized particles. This ability is of primary interest for river survey applications since the long term sediment transfer is believed to be driven by these intense events.

Key words: sediment transport, horizontal ADCPs, multi-frequency acoustics, sediment attenuation

---

* Corresponding author. Tel: +334 72 20 87 65; fax: +334 78 47 78 75.
Email address: stephanie.moore@cemagref.fr (S. A. Moore).

1 INTRODUCTION

Although the use of acoustic Doppler current profilers for horizontal profiling is not novel (see, for example, *Marmorino et al.* (1999)), the commercial development of instruments designed specifically for this purpose occurred within the last five to ten years. As with a traditional vertically-deployed ADCP, the horizontal equivalent is monostatic and monofrequency and the profiling range depends on its carrier frequency, which is typically 300, 600, or 1200 kHz. Horizontal ADCPs (H-ADCPs) are designed to be installed at a fixed location facing horizontally from their mounting structure in order to measure horizontal current profiles. The interest in using horizontal ADCPs for gauging as opposed to the more traditional method with a motor boat and a vertically-oriented ADCP is that H-ADCPs can provide continuous measurements, whereas gauging with a vertically-oriented ADCP is limited to the number of hours per day a person can spend in a boat. If a suitable model exists for calculating discharge from the horizontal profile of velocity, then the combined knowledge of flow velocity and particle concentration (from acoustic intensity) can be used to assess the flux of suspended sediments. The use of classical ADCPs for quantitative measurements of suspended sediment has been discussed by *Holdaway et al.* (1999) and *Reichel and Nachtnebel* (1994) (earlier report for river applications), amongst others. In terms of the application of H-ADCPs to river studies, previous work has focused on their use for discharge measurements in rivers (*Le Coz et al.*, 2008; *Nihei and Kimizu*, 2008; *Hoitink et al.*, 2009), but, to the best of our knowledge, no peer reviewed papers have yet been published on their use for sediment flux measurements. Nevertheless, *Topping et al.* (2007) developed a method for discriminating

sands from silts and clays using intensity profiles collected with side-looking acoustic Doppler profilers in rivers. With data at a single frequency, they determined the concentration of sand sized particles from the backscattered intensity and the concentration of the finer particles from the acoustic attenuation. This method has since been tested at a number of other study sites (e.g. *Wright et al.* (2010) and *Wood* (2010)). The present work differs from that of Topping and his collaborators in a number of ways.

To begin with, the purpose of this paper is to provide potential users of commercial horizontal ADCPs with enough information to be able to decide whether use of the backscattered intensity for inversion to suspended sediment concentration is feasible for a given study site, sediment size and concentration. As a result, many details about our study site and the problems that we encountered are provided. In terms of the acoustic inversion, we focus solely on the inversion of the attenuation data and take an interest in the potential of multi-frequency measurements. Multi-frequency acoustics has been applied successfully in fine-scale flow and sediment transport studies in order to profile sediment size (*Hay and Sheng*, 1992; *Thorne and Hardcastle*, 1997) and sediment fluxes across the highly concentrated benthic flow region (*Hurther et al.*, 2011). As for long range profiling applications, *Topping et al.* (2007) used instruments at multiple frequencies but provided little comparison between the data at the different frequencies.

The field site and instrumentation are presented in Sections 2 and 3, respectively and the acoustic theory is presented in Section 4. The results are presented in three main parts. Section 5.1 is focused on the proper positioning of the instruments and presents a model of the impact of acoustic scattering from the air-water interface on the measured intensity profiles. Section 5.2 dis-

cusses the need for knowledge of the spatial distributions of concentration and grain size and provides an estimate of the detectable range of concentrations for each instrument used in this study. In Section 5.3 we present theoretical estimations of the scattering and attenuation constants for the grain sizes and concentrations encountered at this study site. The major contribution of this study comes in the final section where we present measurements of suspended sediment concentration from multi-frequency acoustic attenuation data, comparing our results to measurements from a calibrated optical turbidity meter.

2 Field Site

2.1 Presentation

The Romans-sur-Isère study site is located on the right bank of the Isère river in the town of Romans-sur-Isère, France. At this location, the river is roughly 90 m wide and the maximum depth is about 4 m. A horizontal cross section of the bathymetry obtained with the bottom tracking function of a 600 kHz RD Instruments Workhorse Rio Grande ADCP is shown in Figure 1.

The site is located between two dams, lying ∼6 km upstream of the La Vanelle dam and ∼2 km downstream of the Pizançon dam. Although the hydraulic and sediment conditions at this site are dependent on the hydrologic regime (precipitation, snow melt), they depend largely on the operations of the neighbouring dams. The upstream dam has the potential to release high amounts of fine sediment during floods and the downstream dam controls the mean water level and hence the mean flow velocity. The mean discharge and particle concentration can exceed 1000 m^3/s and 1 kg/m^3 when the flow is accelerated

during floods or dam opening. However, during these periods the downstream dam is opened wider than usual which results in a decrease in water level; this means that velocity values at this site are more telling of hydrologic conditions than are discharge values. During the majority of the year, mean velocities fluctuate around 1 m/s and suspended sediment concentrations are around 0.01 kg/m^3. Floods at this study site tend to occur during the spring snowmelt or during certain rain storms or dam operations. Concentrations can exceed 1 kg/m^3 during both natural floods and dam flushing events which occur in the summer months on a number of tributaries tens of kilometers upstream.

In order to validate the velocity measurements obtained with the horizontal acoustic Doppler current profilers, a second measure of velocity is required. Continuous discharge measurements are available at the Beaumont Monteux gauging station, 15 km downstream, and local measurements can be made at the site by gauging with a motor boat and a vertically-oriented ADCP.

2.2 Suspended Sediment Spatial Distribution

Unlike many ADCP deployments in oceanography, where vertical gradients of concentration and grain size are observed, for a horizontal river deployment we expect the grain size, composition and concentration to be nearly homogeneous throughout the ensonified volume since the depth of the measuring volume changes little with range. In order to verify the homogeneity of the suspended sediment at the study site, an experiment was performed March 31 2010 during which water samples were collected throughout the river cross-section. During the experiment a Niskin bottle was used to collect 1-l samples of water at depths of 0 m, 1 m, 2 m, 3 m and ranges of 10 m, 30 m, 50 m, 70 m,

and 90 m from the right bank at the along-stream position of the staff gauge. The mean velocity during the experiment was ∼0.8 m/s. Particle concentrations were determined following the ISO standard ISO 11923 (1997). Grain size analysis was performed on these samples using a Hydro 2000G Mastersizer constructed by Malvern Instruments. This instrument is based on the low-angle laser light scattering technique and the Fraunhoffer method is used for our measurements. For the range of primary particle sizes encountered in this study, light scattering is proportional to their projected area. Assuming particle sphericity, the instrument outputs a grain size distribution in terms of the percent of the total volume occupied by grains of each size class. In between sampling and grain size analysis, the samples were stored at 14°C. Since anywhere from a few days to a few months could go by between sample collection and grain size analysis, the samples were disaggregated using ultrasonic waves prior to analysis. This should break up any flocs that may have existed in the original water sample or were formed in the time between sampling and analysis. As such, the grain size distributions that we measured represent the sizes of the primary particles in suspension. We have no information on the mineralogy or biological content of the suspended particulate matter. However, flocculation of the suspended sediment at the study site is a distinct possibility considering clay particles are present and organic content is probable.

The mean concentration for all samples collected throughout the river cross-section was 0.031 kg/m^3 and the standard deviation from the mean was 0.002 kg/m^3, which is the typical uncertainty for the filtration method. No noticeable trend in concentration or grain size was seen with either depth or distance across the river. The volume-fraction size distributions were unimodal with a

median diameter, d_{50}, ranging from 5 to 10 μm. While these results may only be representative of the velocities and concentrations encountered March 31 2010, in the remainder of the analysis it will be assumed that the distributions of grain size and concentration are homogeneous throughout the ensonified volume. The authors believe this to be a fair assumption considering the study site is along a relatively straight and uniform reach of the river and is far from any confluences.

2.3 Grain Size Distributions

In addition to the samples collected March 31 2010, grain size analysis was performed on water samples collected after the peak of the spring flood, between June 1 and June 10 2010 and on samples collected May 11 2010 during a small event for which concentrations rose to 0.1 kg/m^3.

When represented as volume size distributions, the samples collected May 11 have trimodal distributions with modes at d $\approx$ 10 μm, 90 μm and 170 μm. Those collected after the flood had either unimodal or bimodal distributions with peaks at d $\approx$ 10 μm or at d $\approx$ 10 μm and 110 μm. We suspect that samples containing sand-sized particles correspond to samples collected shortly after high shear-stress events which can lead to the resuspension of sediment stocks, however a study of the link between the forms of the grain size distributions and the hydraulic conditions at this site has not yet been undertaken.

Since a variety of distributions were measured for the suspended sediment sampled at Romans-sur-Isère, three representative size distributions will be tested in our theoretical calculations: **(A)** a unimodal; **(B)** a bimodal; and

(C) a trimodal distribution. We calculate an average distribution from three consecutive measurements of two different samples corresponding to each case. Both the volume and number size distributions are depicted in Figure 2. It can be seen that the conversion from volume fraction to number fraction distributions results in narrower distributions and the modes at larger grain sizes are suppressed. This is because relatively few large particles may occupy a large volume.

3 Instrumentation

3.1 Turbidity Meter

A SOLITAX sc optical turbidity meter constructed by Hach Lange is installed at the study site in order to provide a continuous measure of suspended sediment concentration. It is installed at a depth of 0.5 m on the right bank of the river as shown in Figure 3. For all data presented in this article, the turbidity meter was operated in Total Suspended Solids (TSS) mode. This mode of operation is to be used when particle concentrations are high, although the manufacturer does not specify a concentration. While concentrations at this site are typically on the order of 0.01 kg/m^3, the high concentration mode of operation was selected because concentrations may exceed 1 kg/m^3 during floods. The turbidity meter functions by emitting light with a light-emitting diode and detecting the scattered light with a photoreceptor positioned at 140° to the incident direction. The optical turbidity is recorded in units of mg/l TSS (p.9 *Hach Lange*, 2006) and water samples are required in order to relate this unit to mass concentration.

An ISCO 6712 peristaltic pump automatic sampler was installed along the right river bank (see Figure 3). The water intake of the sampler is at the same depth as the optical sensor, 0.5 m, and at the same along-stream position as the 300 kHz H-ADCP. The automatic sampler is linked to the turbidity meter and can be programmed to sample when triggered by events, sampling say once an hour when the turbidity exceeds a certain value. Alternatively, it can be programmed to sample regularly over a fixed time period. When triggered to sample, a plastic bottle is filled with 700 mL of water.

In order to calibrate the turbidity meter, water samples were also collected by hand by submerging 1-l plastic bottles just below the surface. In total, 128 samples were collected between April 2009 and January 2011. In accordance with the ISO standard ISO 11923 (1997), 500 mL of each sample were filtered, dried and weighed in order to determine the mass concentration of particles. Figure 4 is a plot of the concentration of suspended particles versus turbidity at the time of sampling. The concentrations that were measured ranged from 0.0047 kg/m^3 to 8.3 kg/m^3 while the turbidity values encountered ranged from 8.8 mg/l TSS to 8.3 g/l TSS. It can be seen from Figure 4 that a clear linear relationship exists between concentration and optical turbidity over a range of concentration values that spans three orders of magnitude. The samples that correspond to the grain size measurements that were shown in Figure 2 are depicted with different symbols in Figure 4. It can be seen that the turbidity meter is relatively insensitive to the differences in the size distributions of the primary particles that were observed at this study site, at least relative to the other sources of scatter on a log-log plot. What is more, there appeared to be no grouping of the points by events. Thus, in the remainder of our analysis we calculate the concentration of suspended sediment from the turbidity data

using the linear relationship shown in Figure 4. It can be seen, however, that concentration values obtained using this linear relationship will be likely be overestimated when the concentration exceeds 0.2 kg/m^3.

3.2 Acoustic Instruments

The study site is equipped with three RD Instruments H-ADCPs which operate at 307.2 kHz, 614.4 kHz and 1228.8 kHz. They shall be referred to as the 300 kHz, 600 kHz, and 1200 kHz instruments in the remainder of this paper. Beyond the experimental purpose of this installation, the interest in having simultaneous data at various frequencies is that it provides the possibility of determining grain size of the suspended sediment. The 300 kHz instrument is a Workhorse model, the 600 kHz instrument is a Workhorse prototype and the 1200 kHz instrument is a Channel Master H-ADCP. The depth and pitch of installation of each instrument are listed in Table 1 and depicted in Figure 1. The beam width, far field distance and nominal profiling range of each instrument are also listed in Table 1. The beam widths listed are those provided by the manufacturer. In practice, they can differ by a few tenths of a degree. The maximum profiling range of each instrument depends strongly on the concentration of sediment in suspension, as will be seen later in this article, and can easily be increased or decreased by 50% depending on grain size and concentration.

Each instrument is composed of either two or three monostatic piezoelectric transducers. The axis of each transducer and the sound that they emit are often referred to as "beams", in reference to the main beam of the lobed radiation pattern that they transmit. The 300 kHz and 600 kHz instruments

each have three transducers: one points downstream (beam 1), one points upstream (beam 2), and one faces across stream (beam 3). For the 600 kHz instrument, the three transducers are in the same plane and are separated by 30.2°. The axis of the instrument is the axis of beam 3. For the 300 kHz instrument, beam 3 is parallel to, but slightly raised from the plane of beams 1 and 2, which are both at an angle of 20° to the instrument axis. The 1200 kHz instrument has two beams: beam 1 faces 20° downstream and beam 2 faces 20° upstream. The horizontal ADCPs are equipped with temperature sensors in order to calculate the sound celerity. Their sampling rate is typically 2 Hz (*RD Instruments*, 2008).

In order to avoid interference between the various H-ADCPs, they are programmed to ping in turn, with each instrument transmitting 15 pings and then lying dormant until a total of 75 seconds has passed. The profiles of velocity and intensity measured by each transducer are internally averaged and the final result is one profile of intensity and one of velocity for each beam every 75 seconds. The transmit pulse length and size of the range gates that were used corresponded to the manufacturer's recommendations for our specific site. The cell size was 2 m for the 300 kHz H-ADCP, 1 m for the 600 kHz H-ADCP and 0.5 m for the 1200 kHz instrument. In terms of the coordinate system of the velocity measurements, the positive x direction is downstream.

Author-produced version of the article published in Continental Shelf Research (2012), vol.46, p. 50-63
The original publication is available at http://www.sciencedirect.com/ doi : 10.1016/j.csr.2011.10.013

4 Theory

4.1 Acoustic Inversion

In the following analysis we employ the formulations of *Thorne and Hanes* (2002) and *Thorne and Buckingham* (2004) for incoherent scattering from suspensions of sandy sediments as well as the formulations of *Urick* (1948) for sediment attenuation from suspensions of fine particles. For incoherent scattering, the square of the root-mean-square backscattered voltage, V_{rms}, that is detected by a monostatic piston transducer can be written as

$$V_{\mathrm{rms}}{}^2 = \frac{k_s{}^2 k_t{}^2}{\Psi^2 r^2} M e^{-4\alpha r}\,, \tag{1}$$

where

$$k_s^2 = \frac{\langle a_s{}^2 f^2 \rangle}{\rho_s \langle a_s{}^3 \rangle}\,, \qquad k_t{}^2 = p_0{}^2 r_0{}^2 \mathcal{R}^2 T_v{}^2 \frac{3\tau c}{16} \left(\frac{0.96}{k a_t}\right)^2. \tag{2}$$

In the above equations k_s is the sediment backscattering function, k_t is the system constant, r is the range from the transducer to the ensonified volume, Ψ is the near field correction factor (*Downing et al.*, 1995), M is the mass concentration of scatterers and α is the attenuation. In the expression for the system constant k_t, $\mathcal{R}$ is the transducer receive sensitivity, T_v is the voltage transfer function of the system and p_0 is the pressure at the reference distance r_0, which is normally defined as 1 m. The symbol τ is the acoustic pulse duration, c is the speed of sound in water, k is the acoustic wave number and a_t is the radius of the active area of the transducer.

In the expression for the sediment backscattering function k_s, f is the far field form factor which describes the scattering properties of the particles, a_s is the particle radius, ρ_s is the particle density, and angular brackets represent an average over the particle number size distribution. The equation used for the far field form factor f was taken from *Thorne and Meral* (2008). It is expressed in terms of the non-dimensional wave number, $x = ka_s$, as

$$f = \frac{x^2 \left(1 - 0.35e^{-((x-1.5)/0.7)^2}\right) \left(1 + 0.5e^{-((x-1.8)/2.2)^2}\right)}{1 + 0.9x^2}. \tag{3}$$

The attenuation α is the sum of the attenuation due to absorption by the water, α_w, and the attenuation due to the presence of the suspended particles, α_s. We use the expression for α_w that is provided by *Fisher and Simmons* (1977), neglecting the pressure term:

$$\alpha_w = \left(55.9 - 2.37T + 4.77 \times 10^{-2}T^2 - 3.48 \times 10^{-4}T^3\right) 10^{-15} F^2\,, \tag{4}$$

where T is the temperature of water in degrees Celsius and F is the frequency in Hz. The sediment attenuation includes attenuation due to scattering by the particles, $\alpha_{s,\,\mathrm{scat}}$, and viscous absorption in the boundary layer surrounding fine particles, $\alpha_{s,\,\mathrm{visc}}$, both of which are linearly proportional to the mass concentration of scatterers. The scattering attenuation can be written as (*Thorne and Meral*, 2008)

$$\alpha_{s,\,\mathrm{scat}} = \frac{3M \left\langle {a_s}^2 \chi \right\rangle}{4\rho_s \left\langle {a_s}^3 \right\rangle} = M \left\langle \xi_s \right\rangle \tag{5}$$

where

Author-produced version of the article published in Continental Shelf Research (2012), vol.46, p. 50-63
The original publication is available at http://www.sciencedirect.com/ doi : 10.1016/j.csr.2011.10.013

$$\chi = \frac{0.29x^4}{0.95 + 1.28x^2 + 0.25x^4}, \tag{6}$$

ξ_s is what we refer to as the scattering attenuation term and angular brackets again represent an average over the particle number size distribution.

The viscous sediment attenuation $\alpha_{s,\mathrm{visc}}$ can be written as (*Hay*, 1983)

$$\alpha_{s,\,\mathrm{visc}} = M\langle\xi_v\rangle \tag{7}$$

where ξ_v is the viscous absorption term of *Urick* (1948):

$$\begin{aligned} \xi_v &= \frac{k\left(\sigma-1\right)^2}{2\rho_s}\left[\frac{s}{s^2+\left(\sigma+\delta\right)^2}\right] \\ s &= \frac{9}{4\beta a_s}\left[1+\frac{1}{\beta a_s}\right] \\ \sigma = \frac{\rho_s}{\rho_0}, \quad \delta &= \frac{1}{2}\left[1+\frac{9}{2\beta a_s}\right], \quad \beta = \sqrt{\frac{\omega}{2\nu}} \end{aligned} \tag{8}$$

where ω is 2π times the frequency and ν is the kinematic viscosity of water, 1.3×10^{-6} m^2/s. As in Equation 2, the angular brackets denote an average over the number size distribution of the suspended sediment.

Returning now to Equation 1, we see that it is useful when one has direct access to the backscattered signal. However, with the commercial instruments used in this study, we only have access to the processed signal which is output in the manufacturer specified unit of Received Signal Strength Indicator counts. This is not a physical unit, but rather a relative measure of intensity for which the reference pressure is 1 μPa at 1 m. If the ambient noise intensity in counts, E_{noise}, is known, then the received signal intensity in counts, E, can

be converted to the intensity in decibels, I_{dB}, using the following expression from *Gostiaux and van Haren* (2010):

$$I_{\mathrm{dB}} \;=\; 10\log_{10}\left(10^{k_c E/10} - 10^{k_c E_{\mathrm{noise}}/10}\right)\,, \tag{9}$$

where k_c is the count to decibel conversion factor which depends on the temperature of the electronics, T_{e} (°C) in the following manner,

$$k_c = \frac{127.3}{T_{\mathrm{e}} + 273} \tag{10}$$

(*RD Instruments*, 2009, p. 57). Equation 9 is a correction to the commonly used equation of *Deines* (1999) and it is important to use this formulation when the signal to noise ratio is below a factor of ten. The value for E_{noise} that is required in Equation 9 can be obtained either when the profiling range of the instrument is sufficiently long, or when the signal is significantly attenuated due to the presence of scatterers. Noise levels for each transducer of the horizontal ADCPs employed in this study were determined from data obtained during a large flood during which significant attenuation was observed. These values, which are summarized in Table 2, can vary by a couple of counts from event to event.

Based on the data that are available to the user of a commercial ADCP, it is more convenient to rewrite Eq. 1 in terms of pressure,

$${p_{\mathrm{rms}}}^2 = {p_0}^2 {r_0}^2 \,\frac{{k_s}^2 {k_t'}^2}{\Psi^2 r^2}\, M e^{-4\alpha r} \tag{11}$$

modifying the variable k_t in the following manner,

Author-produced version of the article published in Continental Shelf Research (2012), vol.46, p. 50-63
The original publication is available at http://www.sciencedirect.com/ doi : 10.1016/j.csr.2011.10.013

$$k_t{}'^2 = \frac{3\tau c}{16}\left(\frac{0.96}{ka_t}\right)^2. \tag{12}$$

The received signal level in decibels is then obtained by dividing both sides of Equation 11 by the square of a reference pressure, p_{ref}, and taking ten times the logarithm of this result as follows,

$$I_{\mathrm{dB}} \;=\; 10\log_{10}\left(\frac{{p_{\mathrm{rms}}}^2}{{p_{\mathrm{ref}}}^2}\right) \;=\; 10\log_{10}\left(\frac{{p_0}^2{r_0}^2}{{p_{\mathrm{ref}}}^2}\right) + 10\log_{10}\left(\frac{{k_s}^2 k_t{}'^2}{\Psi^2 r^2}\, M e^{-4\alpha r}\right) \tag{13}$$

The reference pressure, p_{ref}, for all RD Instruments ADCPs is 1 μPa and the reference distance r_0 is 1 m. Substituting this value for r_0, we see that the first term on the right hand side of Equation 13 is the term commonly referred to as the source level, SL:

$$SL = 10\log_{10}\left(\frac{{p_0}^2}{{p_{\mathrm{ref}}}^2}\right) \tag{14}$$

(*Clay and Medwin*, 1977). Unfortunately the user of a commercial ADCP does not have access to the source power and thus cannot compute p_0. As a consequence, a direct conversion from the acoustic intensity in counts to the concentration of scatterers in the water is impossible without calibration of the instruments. This highlights the need for complimentary measurements of concentration for installations such as ours, where the instruments were deployed in the field without prior calibration.

One of the objectives of this study was to determine the impact that acoustic scattering from the air-water interface has on the measured intensity and velocity profiles at this particularly shallow study site. In order to avoid interception of the acoustic beams with the central rise in the river bottom (see Figure 1 for bathymetry), the horizontal ADCPs were installed either facing directly across the river, as with the 600 kHz H-ADCP, or tilted slightly upwards, as with the 300 kHz instrument. Looking at the instrument configuration in Figure 1, we see that the main beam of both the 300 kHz and 600 kHz instruments intercept the surface 50 m and 60 m from the right bank, respectively. As a result, we did not expect to have valid measurements across the entire profile, but the data were perturbed at distances much nearer to the instruments than expected when concentrations were low ($\leq \sim 0.03$ kg/m^3). If scattering from the air-water interface were to be detected by the transducers, we would expect to see high intensities and very low and irregular velocities, since capillary waves created by macroturbulence move in all directions. We suspect that when suspended sediment concentrations are low, the signal from the air-water interface may over-power that from the suspended sediment and subsequently bias the results.

In Section 5.1, we model the air-water interface as a Lambertian scatterer of sound. In optics, the radiant intensity (power per unit solid angle) that is observed from a Lambertian surface is proportional to the cosine of the angle θ between the observer's line of sight and the surface normal. In acoustics, the backscattered intensity, I_{bs}, from a Lambertian surface depends on the angle of incidence of the incoming wave, θ, as

Author-produced version of the article published in Continental Shelf Research (2012), vol.46, p. 50-63
The original publication is available at http://www.sciencedirect.com/ doi : 10.1016/j.csr.2011.10.013

$$I_{bs} = \mu \cos^2(\theta)\, I_i\,, \tag{15}$$

where μ is the Lambert parameter which ranges from zero to one and I_i is the incident intensity. The Lambert parameter is a measure of the scattering strength of a rough surface. In oceanographic studies the ocean floor is commonly treated as a Lambertian scatterer. The sea surface has also been modeled as a Lambertian scatterer (e.g. *Davis et al.*, 2002). This is a fair approximation if the length scale of the surface roughness is on the same order as the incident wavelength. Such is the case for our study if we consider the surface roughness to be created by capillary waves: the wavelength of the 300 and 600 kHz signals are 4.9 mm and 2.4 mm, respectively, while the presence of capillary waves with a root-mean-square amplitude of O(1mm) is likely.

The intensity that is incident on the surface is calculated for a given water level and angle of inclination of the instruments based on the directivity patterns of the transducers that are calculated using the beam widths listed in Table 1. The intensity that is incident on the surface, I_i, is related to the directivity, D, the magnitude of the vector between the origin of the transducer and the point of insonification of the surface, R, and the attenuation α as

$$I_i = \frac{I_0 D^2 e^{-2\alpha R}}{R^2} \tag{16}$$

where $I_0 = {p_0}^2 {r_0}^2$. In Figure 5(a) we have plotted the intensity that is incident on the surface relative to I_0 at all ranges, r and angles ϕ for the 300 kHz instrument using the mean water level. The symbol r represents the range along the projection of the acoustic axis onto the surface and ϕ is the angle

between this line and the point of insonification of the surface.

Combining Equations 15 and 16 and accounting for spherical spreading and attenuation of the scattered wave, the intensity that would be detected for scattering from the air-water interface in the cell at distance r_j can be expressed as

$$I_{\text{detected}\,j} = \frac{\mu \cos^2(\theta_j)\, I_0\, e^{-4\alpha R_j}}{{R_j}^4} \sum_{k=-\phi}^{\phi} {D_{j,k}}^4\, r_j dr d\phi, \tag{17}$$

where $D_{j,k}$ is the directivity calculated at range r_j and angle, ϕ_k. Due to the small angle of inclination of the instruments, the range r along the surface is essentially equal to the range along the axis of the transducer which was also represented as r in Equation 1.

5 Results

5.1 The effect of scattering from the air-water interface

In order to test the validity of the velocity measurements made using horizontal ADCPs, river gauging is periodically performed using a vertically-oriented ADCP deployed from a motor boat following the procedure outlined in *Le Coz et al.* (2008) and *Moore et al.* (2009). It was found that during periods of low velocity and concentration (mean velocities $<\sim$ 1 m/s and concentrations on the order of 0.01 kg/m^3), the 300 and 600 kHz H-ADCPs under predicted velocity compared to measurements from ADCP gauging. The 300 kHz instrument severely underestimated the downstream velocity, v_x, in the far half of the river, while the 600 kHz instrument underestimated v_x towards the centre

of the river. To illustrate this, fifteen minutes of data collected by the two instruments during extended periods of (1) relatively low velocity and concentration (maximum velocity of 0.3 m/s and concentration of 0.012 kg/m^3) and (2) relatively high velocity and concentration (maximum velocity of 1.3 m/s and concentration of 0.045 kg/m^3) are shown side by side in Figure 6. The water level for the low velocity and low concentration data was 0.09 m on the staff gauge, while it was 0.20 m for the high concentration and high velocity data. Velocity measurements are shown in the top two panels and intensity measurements are shown in the bottom two panels. The intensity profiles have been corrected for losses due to spreading and attenuation by pure water in order to highlight their irregularities. If the instrument's line of sight was unobstructed, we would expect to see velocity profiles having only positive values (i.e. downstream flow) with minima towards the edges and maxima towards the middle. We would also expect to see constant values of the range corrected intensity for all ranges less than 90 m, which is the distance at which the beams intercept the opposing river bank. This is more or less the case for the data collected when the concentration of suspended sediment was 0.045 kg/m^3 (see Figure 6(b,d)). However, when the concentration of suspended sediment was 0.012 kg/m^3, the velocity and intensity profiles were irregular for both instruments (see Figure 6(a,c)).

The low concentration data shown in Figure 6(a,c) are representative of a large portion of the data collected when the discharge ranged from 100 to 200 m^3/s (mean velocities between 0.30 m/s and 1 m/s) and concentrations ranged from 0.01 to 0.02 kg/m^3. This phenomenon of near-zero velocities and high intensities comes and goes, despite constant values of discharge and concentration. The authors believe this to be the result of scattering from the air-water inter-

face. As mentioned in Section 4.2, we can calculate the theoretical scattering from the air-water interface by treating the surface as a Lambertian scatterer. This is done for the present position and angle of inclination of the 300 and 600 kHz H-ADCPs, ignoring the opposing river bank and the near field of the instruments.

The intensity incident on the surface was computed for the mean water level observed throughout the study period, which was 0.16 m on the staff gauge (see Figure 1 for geometry). The water level at Romans-sur-Isère is fairly stable, typically fluctuating between 0.1 m and 0.4 m during the course of a day. The highest and lowest recorded water levels during the course of our study were 1.63 m and -0.94 m, they were observed before and after a flood which occured at the end of May 2010. Using Equation 17, we calculate the intensity profile that would be measured by the central transducer of each instrument. We could not find any information on the value of the Lambert parameter for scattering from a water-air interface and we do not know the source levels of the transducers used in this study. As such, we assume that the surface roughness parameter μ is one and that the source levels for the 300 kHz and 600 kHz H-ADCPs are 190 dB and 170 dB, respectively. These values were chosen so that the predicted and observed curves could be plotted on the same scale. More realistic parameters might be a μ of 0.002 ($10 \log \mu = -27$ dB) and a source level of 216 dB. The first value is the Lambert parameter that is commonly used for scattering from the ocean floor (e.g. *Ainslie et al.*, 2011; *Ellis*, 2011). The second value is the source level that is given for a RD Instruments 300 kHz Workhorse Navigator DVL on the RD Instruments frequently asked questions website (`http://www.rdinstruments.com/nav_faq.aspx#two`, October, 2011). According to the website, the source level for

a 600 kHz transducer is 217 dB. The combination of these source levels plus the Lambert parameter are very similar to the value that was used for the 300 kHz example, and similar to the value used for the 600 kHz example.

The theoretical intensity profiles are corrected for spreading and attenuation due to water, but the sediment attenuation is neglected in this calculation because it is an order of magnitude less than the attenuation due to water for both instruments when the temperature is 10°C and the particle concentration is 0.010 kg/m^3. The range-corrected theoretical profiles in the far field of the two instruments are depicted in Figure 7(a) for the 300 kHz H-ADCP and Figure 7(b) for the 600 kHz instrument. The wiggles that are seen in the theoretical profiles at ranges less than 50 m for the 300 kHz instrument and ranges less than 20 m for the 600 kHz instrument correspond to the interception of the various side lobes with the surface. The profiles depicted as dashed and dashed-dotted lines in Figure 7 correspond to fifteen minutes of data from extended periods in which the mean velocities were underestimated relative to the discharge velocity. The mean water level for the data depicted as dashed lines in Figure 7 was 0.21 m, while it was 0.09 m for the data depicted as dashed-dotted lines. It can be seen that in the far field of the instruments the theoretical intensities increase with range in a similar manner to the observed profiles. Our ability to reasonably model the effect of scattering from the air-water interface suggests that this technique could be used to determine the ideal depth and inclination for future H-ADCP installations when limited depth is expected to cause problems. Also, we suggest a criterion for data invalidation: if the concentration and size of suspended sediment are expected to be homogeneous across the insonified area, yet the acoustic intensities increase with range, these data should be discarded.

A fair amount of high concentration and high velocity data are available at the Romans-sur-Isère study site. A flood occurred between May 31 and June 1 2010, and shortly thereafter there were a number of natural and man-made events. Unfortunately the turbidity data from the rise of the flood were not properly recorded, but data are available for the descent of the flood and 24 water samples were collected with a time step of 3 hours beginning at 12:02 (UT + 1) June 1 2010. Concentration measurements of these samples show that suspended sediment concentrations reached at least 8 kg/m^3 during the flood. The H-ADCP data collected during this event are used to establish the range of concentrations over which each instrument is sensitive, the caveat being that this may only be valid for the particles encountered at this site during spring snowmelt. The grain size distributions of the particles observed during the descent of the flood had either unimodal or bimodal distributions as previously presented in Section 2.3. In terms of attenuation, we consider that significant attenuation of the 300 and 600 kHz signals occurs when the echo from the left bank decreases below its usual value in low concentration conditions. For the 300 kHz instrument, this value is the saturation level, 222 counts, and for the 600 kHz instrument it is ∼170 counts. Since the maximum profiling range of the 1200 kHz instrument is 30 m, we must look at the entire intensity profiles in order to determine whether or not significant attenuation is occurring. The noise levels of all transducers were previously presented in Table 2. When the intensity of the backscattered signal is at the noise level, no velocity measurements are available. When the intensity is at the saturation level, we have no information about the concentration of sediment

in suspension. The saturation level of the 300 kHz instrument is 222 counts and it is $\sim$ 220 counts for the 600 kHz instrument. Although we have not yet observed saturation of the 1200 kHz instrument, intensities as high as 250 counts have been recorded.

The intensity data collected by the three H-ADCPs throughout the spring flood are shown in Figure 8(a-c); the shading scales are logarithmic and cover the detectable range of each instrument. The intensity values are those measured by beam 3 of the 300 kHz and 600 kHz instruments and by beam 1 of the 1200 kHz instrument. Figure 8(d) is a plot of concentration from the turbidity data for the same time period using the relationship: concentration $= 0.96 \times$ turbidity.

Using the turbidity data as a timeline of the hydrological events, we see that the 300 kHz data in Figure 8(a) are saturated prior to the rise of the flood for all ranges less than $\sim$60 m. The saturation level for beam 3 of the 300 kHz instrument is 222 counts. Once the concentration exceeds ~ 0.5 kg/m^3, around 12:00 May 31, we begin to see noticeable attenuation of the 300 kHz echo intensity. However, due to the relatively low attenuation of the 300 kHz signal compared to the other two instruments, the echo intensity was sufficiently high that velocities could be measured out to a range of 25 m (i.e. the backscattered intensity was above the noise level) as long as the concentration was less than 7 kg/m^3.

During a relatively low amplitude turbidity event that was recorded May 11 2010, the onset of attenuation of the 300 kHz signal occurred at a much lower value of turbidity: it began when the turbidity first exceeded 90 mg/l TSS and continued until the turbidity dropped below 60 mg/l TSS. The difference in

the turbidity value at which attenuation first began for the two events may be related to grain size, since larger particles were seen in water samples collected May 11 2010 (Figure 2(e,f)) than during the flood (Figure 2(a - d)). The role played by grain size in acoustic scattering and attenuation shall be discussed in detail in Section 5.3.

For the 300 kHz instrument, signal attenuation by the suspended sediment does not appear to hinder velocity measurements at this study site unless concentrations exceed 5 kg/m^3. However, the instrument's extreme sensitivity to concentration poses a problem for sediment transport measurements, since a value of concentration cannot be obtained when the echo is saturated. Throughout the study period, it was found that whenever turbidity exceeded $\sim$100 mg/l TSS, the echo was saturated at all ranges less than 60 m. Although we were unaware at the time of measurement, the receiver gain of RD Instruments Workhorse H-ADCPs can be reduced by 40 dB, which is equivalent to $\sim$90 counts (*RD Instruments*, 2008, p. 165). The reduced gain setting was tested with success on September 21 2010 and it was determined that if one's objective is to use a 300 kHz H-ADCP for sediment concentration profiling, the reduced gain setting could be used.

Sediment attenuation of the 600 kHz signal began before the start of the data set that is shown in Figure 8(b). Based on data not shown here, the onset of attenuation occurred when the concentration first exceeded 0.045 kg/m^3. This was true of both the lead-up to the flood May 30 2010 and of the May 11th event. Although attenuation begins at fairly low concentrations, intensity values remain sufficiently high so that the instrument can be used to measure velocities out to 25 meters for all concentrations less than 3 kg/m^3. Unlike the 300 kHz instrument, the onset of signal saturation and attenuation tend

to manifest themselves at the same value of concentration so that saturation only occurs in the first few measurements cells (see dark red zones of Figure 8(b)).

Looking at Figure 8(c), we see that the signal detected by the 1200 kHz instrument did not saturate during this major flood, but this may indicate that attenuation was occurring before the first depth cell. We see that the maximum profiling range at the start of this event is greater than 30 m, but once the concentration exceeds 0.4 kg/m^3 at 12:00 May 31, the instrument's maximum profiling range is reduced due to significant sediment attenuation. Significant attenuation can be seen throughout most of June 1, since the intensity is at the instrument's noise level beyond a few meters from the instrument. According to the manufacturer, the typical profiling range of a 1200 kHz Channel Master H-ADCP should be 15 m for the settings used at this study site; valid measurements of velocity were obtained out to 15 m for all concentration values less than 1.75 kg/m^3. Beyond this value, the attenuation due to the sediment was high, and when concentration exceeded 5 kg/m^3, the measurable range was reduced to less than 6 m from the instrument. While intensity values did not reach the instrument's saturation level during the flood (the maximum intensity observed in cell 1 was 220 counts), they reached 250 counts during the May 11th event. Again, this may be related to different grain sizes of the suspended sediment.

The data presented in this section provide an idea of the range of sensitivity of each instrument to concentration for the particles encountered in our study. First of all, we find that although the 600 kHz and 1200 kHz signals may be attenuated at large ranges when concentrations are on the order of 1 kg/m^3, cells close to the instrument can be used to provide a measure of

concentration. Secondly, it can be seen that although the 300 kHz H-ADCP can be used to measure velocities at longer ranges, when using the default receiver gain setting the signal saturates very easily and the measurable range of concentration is reduced compared to those of the 600 kHz and 1200 kHz instruments. Fortunately, this signal saturation can be avoided by using the reduced receiver gain setting.

5.3 Theoretical estimations of backscatter and attenuation

If we recall the expression for the backscattering term ${k_s}^2$ that was given in Equation 2, we see that it depends on both ${a_s}^2$ and ${a_s}^3$. The ${a_s}^2$ in the numerator comes from the scattering cross section of the particles and this a_s should therefore be the radius of a sphere with the same projected area as the grains. The $\langle {a_s}^3 \rangle$ in the denominator comes from the average particle volume and this a_s should therefore be the radius of a sphere of equivalent volume. In this study, grain size was measured using laser diffraction. For homogeneous spherical grains much larger than the wavelength of the incident light (632 nm for the Helium-Neon laser used by the Malvern laser sizer), the light that is diffracted depends on the geometric cross section, or ${a_s}^2$ (*Wedd*, 2003). As this is our only measure of grain size, the laser diffraction size distributions shall be used in all calculations.

The scattering constant ${k_s}^2$, scattering sediment attenuation term, $\langle \xi_s \rangle$ and viscous sediment attenuation term $\langle \xi_v \rangle$ have been computed for the three grain size distributions measured in water samples at Romans-sur-Isère and previously presented in Section 2.3. Equations 2 and 3 are used to calculate ${k_s}^2$, Equations 5 and 6 are used to calculate $\langle \xi_s \rangle$ and Equation 8 is used to

calculate $\langle \xi_v \rangle$. These results are summarized in Table 3, along with results for a suspension of particles with a single size, $a_s = 0.64\ \mu m$, which corresponds to the mean radius of the unimodal grain size distribution. Values are calculated for the operating frequencies of the three H-ADCPs.

The importance of including both the form and width of a grain size distribution in the calculation of the ensemble scattering parameters has been previously discussed by *Moate and Thorne* (2009). From Table 3 we see that, for a given frequency, the values of the scattering function and the attenuation due to scattering are quite sensitive to the differences in the grain size distributions encountered at Romans-sur-Isère. This is because larger particles play an important role in scattering: as modes at large grain sizes appear, the scattering is greatly increased. The viscous attenuation constant, on the other hand, is fairly insensitive to the differences in grain size that were observed. This is because the particles that exist in the secondary and tertiary modes of the grain size distributions do not contribute to viscous absorption. It can also be seen from Table 3 that the attenuation due to viscous absorption in the boundary layer surrounding the particles dominates that due to scattering from the particles. This is as expected since the grain size distributions are dominated by silt-sized particles. From the values listed in Table 3, we can see that higher concentrations of sand sized particles would increase the backscattering function and hence the backscattered intensity, while higher concentrations of silts and clays would increase the attenuation. This phenomenon was exploited by *Topping et al.* (2007) in their work on measurements of suspended sediment concentration in rivers using side-looking ADCPs.

The difference in intensity that would be recorded for scattering from two different suspensions at a given distance r, can be expressed as:

Author-produced version of the article published in Continental Shelf Research (2012), vol.46, p. 50-63
The original publication is available at http://www.sciencedirect.com/ doi : 10.1016/j.csr.2011.10.013

$$I_{dB2} - I_{dB1} = 10 \log_{10} \left(\frac{M_2 {k_{s2}}^2}{M_1 {k_{s1}}^2} \right) + \frac{40r}{\ln(10)} (\alpha_1 - \alpha_2) \tag{18}$$

where I_{dB1} and I_{dB2} are the theoretical intensities recorded in decibels for suspensions 1 and 2. This difference is converted to counts using a conversion factor of 0.43 dB/count, which is the value at 20°C. For two suspensions with the same concentration but different grain sizes, the second term in Equation 18 is simply the difference of their attenuation constants. Since viscous attenuation dominates scattering attenuation for the unimodal, bimodal and trimodal distributions presented in Table 3, and since the differences between their viscous attenuation constants are small, it can be seen that differences in the backscattered intensity are primarily controlled by the first term in Equation 18 when concentration are low.

Comparing the trimodal distribution to the unimodal distribution, we calculate that the backscattered intensity from a suspension of particles with a trimodal distribution is 20 counts higher than that from particles with a unimodal distribution for the 300 kHz instrument at a range r of 100 m and a concentration of 0.010 kg/m^3. When concentrations are 1 kg/m^3, the difference is only 12 counts since the attenuation terms are no longer negligible. The difference between $I_{dB,\,\mathrm{tri}}$ and $I_{dB,\,\mathrm{uni}}$ for the 600 kHz instrument at 100 m ranges from 20 counts for 0.010 kg/m^3 to 4 counts for 1 kg/m^3. For the 1200 kHz instrument, the difference is 19 counts at 100 m and 0.010 kg/m^3, but when the concentrations reach 1 kg/m^3, the difference is -5 counts, meaning that the backscatter from the unimodal distribution is higher than that from the trimodal distribution. From these values we see that when concentrations of suspended sediment are low (on the order of 0.01 kg/m^3), and thus the at-

tenuation is minimal, the difference between the backscattered intensity from suspensions with trimodal and unimodal distributions is essentially the same for all instruments. This is because we are in the Rayleigh regime ($x << 1$). In the Rayleigh regime, the form function depends only on x^2, meaning that the first term on the left hand side of Equation 18, $10\log_{10}\left({k_{s2}}^2/{k_{s1}}^2\right)$, becomes $10\log_{10}\left(\langle {a_{s2}}^6\rangle \langle {a_{s1}}^3\rangle / \langle {a_{s1}}^6\rangle \langle {a_{s2}}^3\rangle\right)$, which is independent of frequency.

5.4 Field measurements of sediment attenuation

Using the intensity profiles from one beam of each instrument, we can calculate the observed sediment attenuation. For a given time step and given transducer, the attenuation between ranges r_1 and r_2 (both in the far field) can be expressed as

$$\alpha = \left[I_{dB}|_{r_2} - I_{dB}|_{r_1} + 20\log_{10}\left(\frac{r_2}{r_1}\right)\right]\frac{\ln(10)}{40\,(r_1 - r_2)}. \tag{19}$$

As with the previously presented results, we average the intensity data over 15 minutes in order to reduce noise and file size. For the calculation of attenuation, we use cells separated by 2-m for all instruments, as this corresponds to the cell size of the 300 kHz H-ADCP. This means that the attenuation is calculated between cells n and $n+2$ for the 600 kHz instrument (bin size of 1 m) and betweens cells n and $n+4$ for the 1200 kHz instrument (bin size of 0.5 m). From each profile of intensity, we obtain a profile of observed attenuation. The attenuation for pure water is then subtracted from these values using the expression given in Equation 4 and the temperature recorded by the H-ADCPs.

As the sediment size and concentration are assumed to be homogeneous across the insonified volume, we would expect the sediment attenuation to be a constant value across the profile. However, due to the local increases in amplitude of the 300 and 600 kHz signals caused by scattering from the air-water interface at certain ranges, this is not the case. As such, we discard all points for which the intensity increases with range (i.e. all points for which the observed "attenuation" is negative) and use only the data collected within the first 50 m from the 300 and 600 kHz instruments. The average sediment attenuation for each profile is calculated as the mean of all values greater than one half the maximum value for that profile. This is done because low relative values of α are more indicative of suspicious intensity data than are high relative values of α.

In Figure 9 we show the relationships between sediment attenuation and concentration that are obtained for the three H-ADCPs for two events during which particle concentrations exceeded 1 kg/m^3. The turbidity time series for these events are shown in the top two panels of Figure 9: the first event was associated with dam flushing $\sim$200 km upstream and did not correspond to increased velocities; the second event was the spring flood event discussed in Figure 8. The relationships between sediment attenuation and concentration (from turbidity) for these two events are shown in Figures 9 (c) and (d).

Clear linear relationships are seen between attenuation and concentration for all instruments for the two events. The solid lines traced in Figures 9(c) and (d) are the least-squares linear fits to the data. The slopes of these lines are listed in Table 4, as are the values of R^2, the square of the correlation coefficient between the data and the fits. Since $\alpha_s = M\left(\langle\xi_v\rangle + \langle\xi_s\rangle\right) = M\langle\xi_{\mathrm{exp}}\rangle$, these slopes give us what we refer to as the observed sediment attenuation constant,

$\langle \xi_{\rm exp} \rangle$, where "exp" refers to experimental.

The fact that there are such clear linear relationships between sediment attenuation and suspended sediment concentration for a given event implies that the grain size and composition were likely homogeneous throughout each event. The slight differences in the slopes between events suggest that grain sizes may have been slightly different for the two events, however we do not have water samples for the June 30 event in order to confirm this hypothesis. It can be seen that the values of $\langle \xi_{\rm exp} \rangle$ are in good agreement with the theory of Urick for attenuation due to viscous absorption by fine particles (see values of $\langle \xi_v \rangle$ in Table 3). This is especially true of the data from the spring flood for which the experimental values are within a factor of two of the theoretical values. The better agreement between data and theory for the spring flood is likely because the unimodal and bimodal grain size distributions for which the theoretical values were calculated were measured in water samples collected during this event. It can also be seen that the agreement between observations and theory is best for the 300 kHz data and worst for the 1200 kHz data for both events.

Using the linear relationships between sediment attenuation and concentration that are shown in Figure 9(c,d), we can reconstruct a time series of the suspended sediment concentration from the time series of the values of α_s that were measured during these events. This is especially interesting for the spring flood, since a large percentage of the turbidity data were lost on the rise of the flood. We obtain the results that are plotted in Figure 10 for the 300 kHz (circles), 600 kHz (squares) and 1200 kHz (triangles) H-ADCPs. From Figure 10(a), we see that the pronounced peak in turbidity that was observed June 30 can be properly reconstructed using the attenuation data from all H-ADCPs.

The noisiness in the concentration time series from the 300 kHz data before and after the event is due to the insignificant attenuation of the 300 kHz signal when concentrations are less than 0.2 kg/m^3. Overall, there is very good agreement between the optical and acoustical data in terms of amplitude and duration of the event.

There is also very good agreement between the optical and acoustical data for the spring flood (Figure 10(b)) during the periods for which we have simultaneous data, even on small time scales. Take for example the striking agreement for the peak in concentration that occurred between 1:00 and 3:00 June 2. We are able to reconstruct a concentration time series for the period of missing turbidity data and there is very good agreement between the 600 and 1200 kHz predictions throughout this period. Nonetheless, the 300 kHz instrument tends to underestimate concentration between 00:00 and 08:00 June 1 compared to the other two H-ADCPs. This may indicate that there was a temporary change in grain sizes to which the higher frequency instruments were more sensitive. This includes the possibility of the presence of flocs.

Water samples were collected on the fall of the spring flood between June 1, 2010 and June 4, 2010. The concentration values measured by filtration are shown as plus signs in Figure 10(b). It can be seen that both the optical and acoustical data over-predict the concentration compared to the actual concentrations by between 10 and 30%. We remind the reader that the grain size distributions measured for the water samples collected on the fall of the flood were those presented in Figures 2(a-d), i.e. either unimodal or bi-modal. Since there is negligible contribution to the attenuation from sand-sized particles, we would have expected the concentration from the acoustic attenuation data to be less than the actual concentration. However, the inversion of the atten-

uation data is based on a linear relationship between the turbidity data and the attenuation data and, as previously stated, concentrations from turbidity are typically over-estimated when the concentration exceeds 0.2 kg/m^3. This appears to have compensated for the anticipated underestimation of concentartion. Nevertheless, the reader must keep in mind that concentration estimates based on attenuation data alone are likely to be underestimated if the distributions are multimodal. Hence the interest in using attenuation data to obtain concentration of silts and backscattered data to obtain concentrations of sands as was done by *Topping et al.* (2007).

6 Conclusions

The present work was intended as a feasibility study for the application of commercial horizontal ADCPs to sediment flux measurements in rivers. Results were presented from a study site that is equipped with horizontal ADCPs operating at 300, 600 and 1200 kHz. It was found that during low flow conditions the measurements of both the 300 kHz and 600 kHz H-ADCPs were perturbed due to improper positioning: intensity values were seen to increase with range instead of decreasing, and the corresponding velocity values were near-zero. We were able to mimic these intensity profiles by modeling the effects of scattering from the air-water interface. This result has implications for future studies because it shows that in-situ tests on the ideal positioning of an instrument may not be sufficient when the depth is limited: if the tests are performed on a day when suspended sediment concentrations are high, the effects of scattering from the surface may not be noticeable. Also, many users purchase commercial horizontal ADCPs believing that their range of opera-

tion is determined solely by the aspect ratio of the study site, but our results show that this may be too simplistic a rule. Our results imply that the optimal installation depth and inclination of an instrument could be determined prior to installation using this simple modeling technique.

Data collected during two floods associated with high turbidity events were used to determine the relationship between sediment attenuation and suspended scatterer concentrations. Clear linear relationships were established for all acoustic instruments and it was found that attenuation values were in agreement with the theory for viscous absorption from fine particles. Using the observed relationships between sediment attenuation and concentration, we were able to reconstruct the concentration data for a 24-hour period on the rise of the spring flood for which the turbidity data were missing. For periods during which we had both optical and acoustical data, agreement between the two concentration time series was striking, even on short time scales.

The results of this study show that the proposed attenuation method offers great potential for continuous surveys of suspended sediment fluxes in rivers with commercial H-ADCPs. It is particularly adapted to extreme flow events such as floods for which, in the present study, the concentrations were in the g/l (kg/m^3) range. There is, however, the possibility that this method could underestimate the sediment transport in the case of multimodal size distributions with a mode in the sand-sized range. Perspectives for this application include the possibility of determining the effective grain size of the particles in suspension by comparing the sediment attenuation constants obtained for the H-ADCPs of various frequencies.

Acknowledgements

This work was financed by the Compagnie Nationale du Rhône (CNR), Electricité de France (EDF) and the Observatoire des Sédiments du Rhône (OSR). We thank the CNR for the use of their study site and instruments. We thank Teledyne RD Instruments Europe for the loan of two of the three horizontal ADCPs. We would like to thank Guillaume Dramais, Laurent Dramais, Mickaël Lagouy, and Fabien Thollet (Cemagref) for their help with field work and filtration. We also thank Gilles Pierrefeu and Xavier Martin (CNR) for useful discussions and technical support. We thank Alex Hay (Dalhousie University) for his help with the work on Lambertian scattering. We are grateful to the anonymous reviewers and guest editor for their useful feedback.

References

Ainslie, M. A., C. H. Harrison, and M. Zampolli, An analytical solution for signal, background and signal to background ratio for a low frequency active sonar in a Pekeris waveguide satisfying Lambert's rule, in *Proc. 4th International Conf. and Exhibition on Underwater Acoustic Measurements: Technologies and Results*, pp. 491 – 498, 2011.

Clay, C. S., and H. Medwin, *Acoustical Oceanography: Principles and Applications*, John Wiley and Sons, Toronto, 1977, p. 82.

Davis, B. J., P. Gough, and B. Hunt, Sea surface simulator for testing a synthetic aperture sonar, in *Impact of littoral environmental variability on acoustic predictions and sonar performance*, edited by N. G. Pace and F. B. Jensen, pp. 473–480, Kluwer Academic Publishers, The Netherlands, 2002.

Deines, K. L., Backscatter estimation using broadband acoustic Doppler cur-

rent profilers, *Proceeding of the IEEE, 6th working conference on current measurement, San Diego, CA, U.S.A.*, 1999.

Downing, A., P. D. Thorne, and C. E. Vincent, Backscattering from a suspension in the near field of a piston transducer, *J. Acoust. Soc. Am*, *97*, 1614–1620, 1995.

Ellis, D. D., Solutions to range-dependent reverberation and sonar workshop problems using an adiabatic normal mode model, in *Proc. 4th International Conf. and Exhibition on Underwater Acoustic Measurements: Technologies and Results*, pp. 485 – 490, 2011.

Fisher, F. H., and V. P. Simmons, Sound absorption in sea water, *J. Acoust. Soc. Am.*, *62*, 558 – 564, 1977.

Gostiaux, L., and H. van Haren, Extracting meaningful information from uncalibrated backscattered echo intensity data, *Journal of Atmospheric and Oceanic Technology*, *27*, 943–949, 2010.

Hach Lange, Solitax sc user manual, 2006.

Hay, A. E., On the remote acoustic detection of suspended sediment at long wavelengths, *J. Geophys. Res.*, *88*, 7525–7542, 1983.

Hay, A. E., and J. Sheng, Vertical profiles of suspended sand concentration and size from multifrequency acoustic backscatter, *J. Geophys. Res.*, *97*, 15,661 – 15,677, 1992.

Hoitink, A. J. F., F. A. Bushman, and B. Vermeulen, Continuous measurements of discharge from a horizontal acoustic Doppler current profiler in a tidal river, *Water Resour. Res.*, *45*, W11,406, 2009.

Holdaway, G. P., P. D. Thorne, D. Flatt, S. E. Jones, and D. Prandle, Comparison between ADCP and transmissometer measurements of suspended sediment concentration, *Cont. Shelf Res.*, *19*, 421–441, 1999.

Hurther, D., P. D. Thorne, M. Bricault, J-. M. Barnoud, and U. Lemmin,

A multi-frequency Acoustic Concentration and Velocity Profiler (ACVP) for boundary layer measurements of fine-scale flow and sediment transport processes, *Coastal Eng.*, *58*, 594 – 605, 2011.

Le Coz, J., G. Pierrefeu, and A. Paquier, Evaluation of river discharges monitored by a fixed side-looking Doppler profiler, *Water Resour. Res.*, *44*, W00D09, 2008.

Marmorino, G. O., C. L. Trump, and Z. R. Hallock, Near-surface current measurements using a ship-deployed "horizontal" ADCP, *J. Atmos. Oceanic Technol.*, *16*, 1456 – 1463, 1999.

Moate, B. D., and P. D. Thorne, Measurements and inversion of acoustic scattering from suspensions having broad size distributions, *J. Acoust. Soc. Am*, *126*, 2905–2917, 2009.

Moore, S. A., J. Le Coz, G. Pierrefeu, C. Perret, D. Hurther, and A. Paquier, Measuring river flow using sidelooking acoustic Doppler current profilers: a comparison to vertically–oriented ADCP results, in *Proceedings of the 33rd IAHR Congress: Water Engineering for a Sustainable Environment, Vancouver*, 2009.

Nihei, Y., and A. Kimizu, A new monitoring system for river discharge with horizontal acoustic Doppler current profiler measurements and river flow simulation, *Water Resour. Res.*, *44*, W00D20, 2008.

RD Instruments, Workhorse H-ADCP operational manual, 2008, p. 87 and p. 158.

RD Instruments, WinRiver II user's guide, 2009.

Reichel, G., and H. P. Nachtnebel, Suspended sediment monitoring in a fluvial environment: Advantages and limitations applying an Acoustic Doppler Current Profiler, *Water Research*, *28*, 751–761, 1994.

Thorne, P. D., and M. J. Buckingham, Measurements of scattering by sus-

pensions of irregularly shaped sand particles and comparison with a single parameter modified sphere model, *J. Acoust. Soc. Am.*, *116*, 2876–2889, 2004.

Thorne, P. D., and D. M. Hanes, A review of acoustic measurement of small-scale sediment processes, *Cont. Shelf Res.*, *22*, 603–632, 2002.

Thorne, P. D., and P. J. Hardcastle, Acoustic measurements of suspended sediments in turbulent currents and comparison with *in-situ* samples, *J. Acoust. Soc. Am.*, *101*, 2603 – 2614, 1997.

Thorne, P. D., and R. Meral, Formulations for the scattering properties of suspended sandy sediments for use in the application of acoustics to sediment transport processes, *Cont. Shelf Res.*, *28*, 309–317, 2008.

Topping, D. J., S. A. Wright, T. S. Melis, and D. M. Rubin, High-resolution measurements of suspended-sediment concentration and grain size in the Colorado River in Grand Canyon using a multi-frequency acoustic system, in *Proceedings of the 10th International Symposium on River Sedimentation. August 1–4, Moscow, Russia*, 2007.

Urick, R. J., The absorption of sound in suspensions of irregular particles, *J. Acoust. Soc. Am*, *20*, 283 – 289, 1948.

Wedd, M. W., Determination of particle size distributions using laser diffraction, *Tech. rep.*, Educational Resources for Particle Technology, 2003.

Wood, M. S., Evaluation of sediment surrogates in rivers draining to Lower Granite Reservoir, ID and WA, in *Proceedings of the 9th Federal Interagency Sedimentation Conference*, Las Vegas, U.S.A., 2010.

Wright, S. A., D. J. Topping, and C. A. Williams, Discriminating silt-and-clay from suspended-sand in rivers using side-looking acoustic profilers, in *Proceedings of the 9th Federal Interagency Sedimentation Conference*, Las Vegas, U.S.A., 2010.

Author-produced version of the article published in Continental Shelf Research (2012), vol.46, p. 50-63
The original publication is available at http://www.sciencedirect.com/ doi : 10.1016/j.csr.2011.10.013

Table 1

A summary of the depth and pitch of installation of the horizontal ADCPs. Depth is given with respect to the zero on the staff gauge and positive values of pitch indicate upward inclination. The beam width (β) and nominal maximum profiling range of each instrument are also given, based on information provided by the manufacturer. Beam width corresponds to the full width half maximum of the directivity squared (-3dB level of the transmitted power). The distance to the far field of each instrument is also listed.

Instrument	depth (m)	pitch (°)	max range (m)	β (°)	distance to the far field (m)
300 kHz	-2.16	1.8	250	1	12.8
600 kHz	-0.36	0.1	85	1.2	4.5
1200 kHz	-0.76	0.1	15	1.5	2.2

Table 2

A summary of the noise levels measured for each beam of the H-ADCPs used in this study.

Instrument	Beam 1 (counts)	Beam 2 (counts)	Beam 3 (counts)
300 kHz	67	65	68
600 kHz	66	69	68
1200 kHz	35	34	–

Author-produced version of the article published in Continental Shelf Research (2012), vol.46, p. 50-63
The original publication is available at http://www.sciencedirect.com/ doi : 10.1016/j.csr.2011.10.013

Table 3. Values of the scattering function ${k_s}^2$, the scattering attenuation function $\langle \xi_s \rangle$ and the viscous attenuation function $\langle \xi_v \rangle$ computed for the various grain size distributions presented in Figure 2 using Equations 2 - 8.

	307.2 kHz			614.4 kHz			1228.8 kHz		
Distribution	${k_s}^2$ (m^2/kg)	$\langle \xi_s \rangle$ (m^2/kg)	$\langle \xi_v \rangle$ (m^2/kg)	${k_s}^2$ (m^2/kg)	$\langle \xi_s \rangle$ (m^2/kg)	$\langle \xi_v \rangle$ (m^2/kg)	${k_s}^2$ (m^2/kg)	$\langle \xi_s \rangle$ (m^2/kg)	$\langle \xi_v \rangle$ (m^2/kg)
single size	4.9×10^{-10}	7.2×10^{-11}	0.043	7.9×10^{-9}	1.2×10^{-9}	0.113	1.3×10^{-7}	1.8×10^{-8}	0.254
unimodal	3.7×10^{-6}	5.4×10^{-7}	0.033	5.9×10^{-5}	8.6×10^{-6}	0.088	9.4×10^{-4}	1.4×10^{-4}	0.213
bimodal	1.9×10^{-5}	2.7×10^{-6}	0.035	3.0×10^{-4}	4.2×10^{-5}	0.091	4.4×10^{-3}	6.3×10^{-4}	0.215
trimodal	2.8×10^{-5}	4.0×10^{-6}	0.035	4.4×10^{-4}	6.2×10^{-5}	0.092	6.1×10^{-3}	8.8×10^{-4}	0.219

Author-produced version of the article published in Continental Shelf Research (2012), vol.46, p. 50-63
The original publication is available at http://www.sciencedirect.com/ doi : 10.1016/j.csr.2011.10.013

Table 4

Slope of the least-squares linear regressions between sediment attenuation and suspended sediment concentration from turbidity (i.e. the experimental sediment attenuation constant $\langle \xi_{\text{exp}} \rangle$) for the data presented in Figure 9.

Instrument	Slope for June 30 2010	R^2	Slope for Flood 2010	R^2
300 kHz	0.017	0.86	0.030	0.98
600 kHz	0.034	0.96	0.053	0.99
1200 kHz	0.075	0.99	0.115	0.99

Author-produced version of the article published in Continental Shelf Research (2012), vol.46, p. 50-63
The original publication is available at http://www.sciencedirect.com/ doi : 10.1016/j.csr.2011.10.013

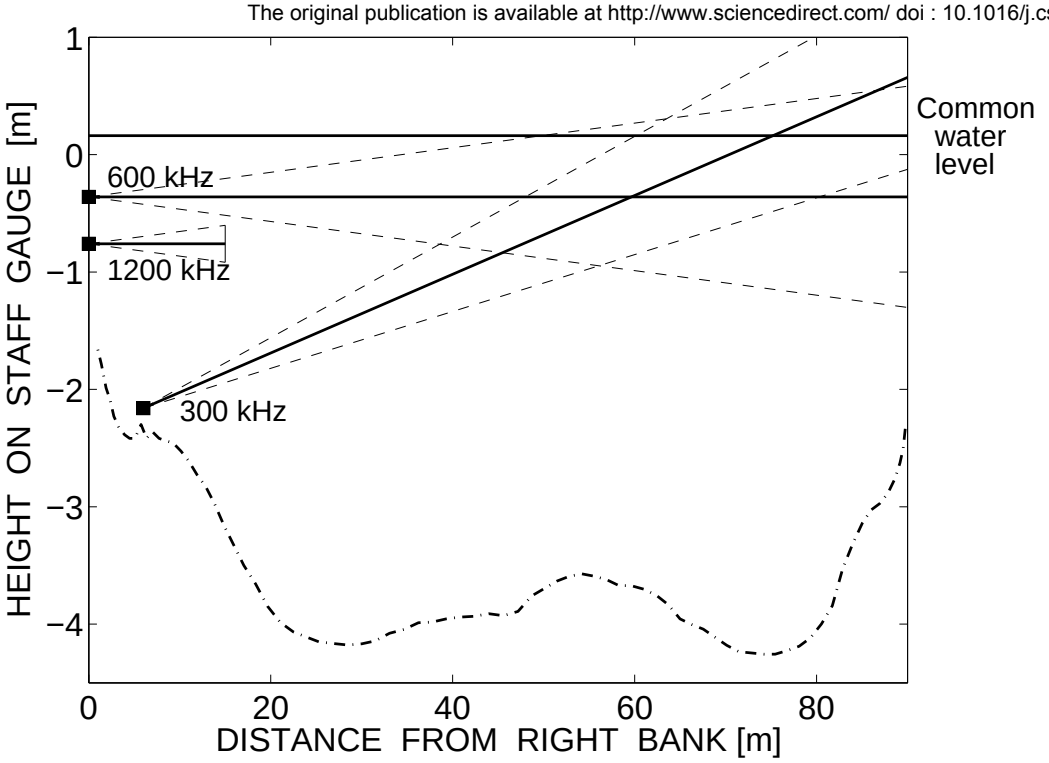

Fig. 1. Upstream view of the Romans-sur-Isère study site. The solid horizontal line at 0.14 m indicates a typical water level and the dashed-dotted line is the river bathymetry. The horizontal ADCPs are indicated as squares. The solid lines represent the projections of the "central" beam of each instrument and dashed lines represent their beam widths (-3dB level of the transmitted power).

Author-produced version of the article published in Continental Shelf Research (2012), vol.46, p. 50-63
The original publication is available at http://www.sciencedirect.com/ doi : 10.1016/j.csr.2011.10.013

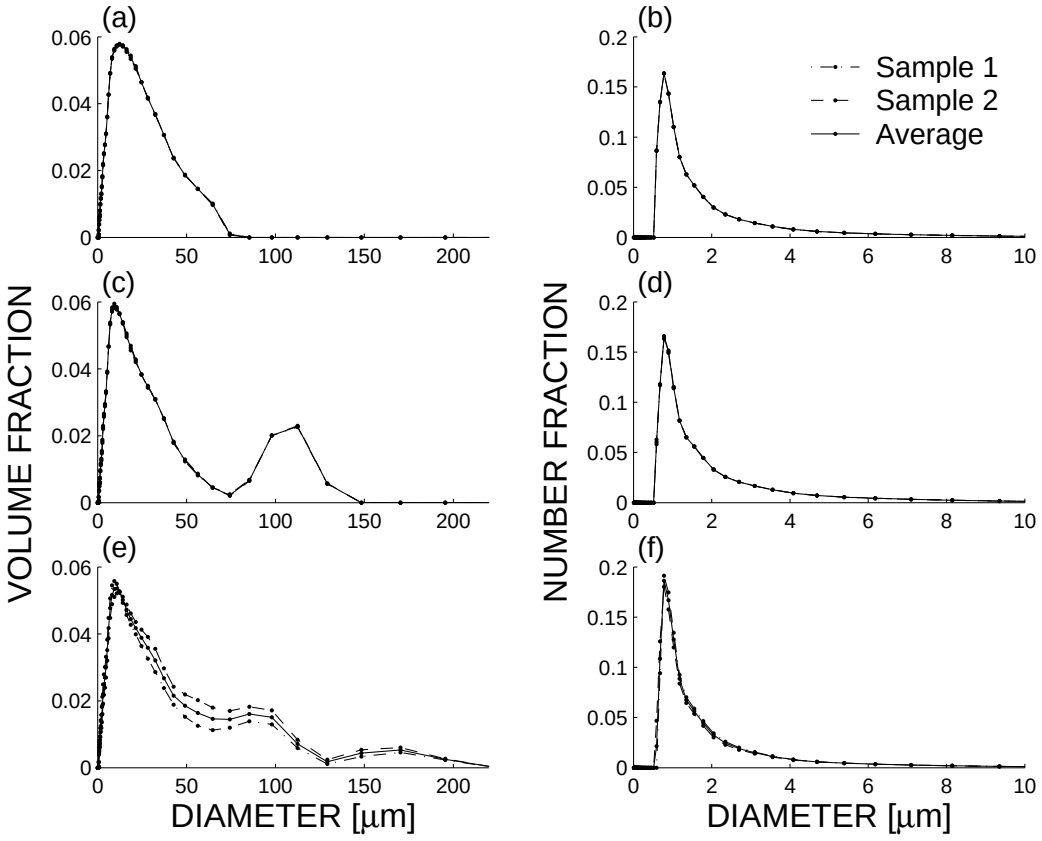

Fig. 2. Grain size distributions measured using laser diffraction spectroscopy. The data are represented as volume fraction (a,c,e) and number fraction (b,d,f) distributions with (a,b) being the unimodal case, (c,d) the bimodal case, and (e,f) the trimodal case. The dashed and dashed-dotted lines correspond to the measured distributions of two samples (each the average of three runs), and the solid lines are their average. In cases where the two distributions are very similar, the individual curves are not discernible.

Author-produced version of the article published in Continental Shelf Research (2012), vol.46, p. 50-63
The original publication is available at http://www.sciencedirect.com/ doi : 10.1016/j.csr.2011.10.013

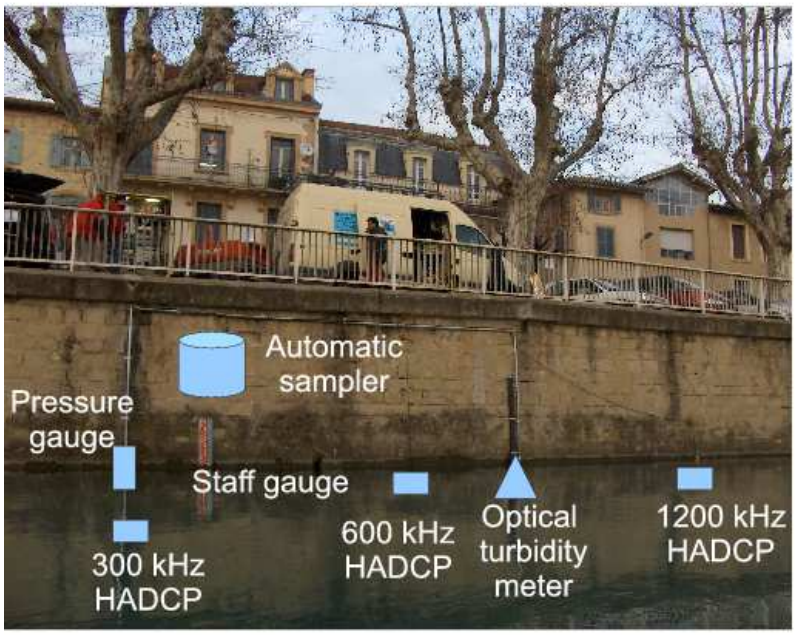

Fig. 3. The Romans-sur-Isère study site. All instruments are installed along the wall of the right bank except the 300 kHz H-ADCP which is attached to a 6-m long arm. To give an idea of scale, the thick vertical bars of the railing are separated by 2 m.

Author-produced version of the article published in Continental Shelf Research (2012), vol.46, p. 50-63
The original publication is available at http://www.sciencedirect.com/ doi : 10.1016/j.csr.2011.10.013

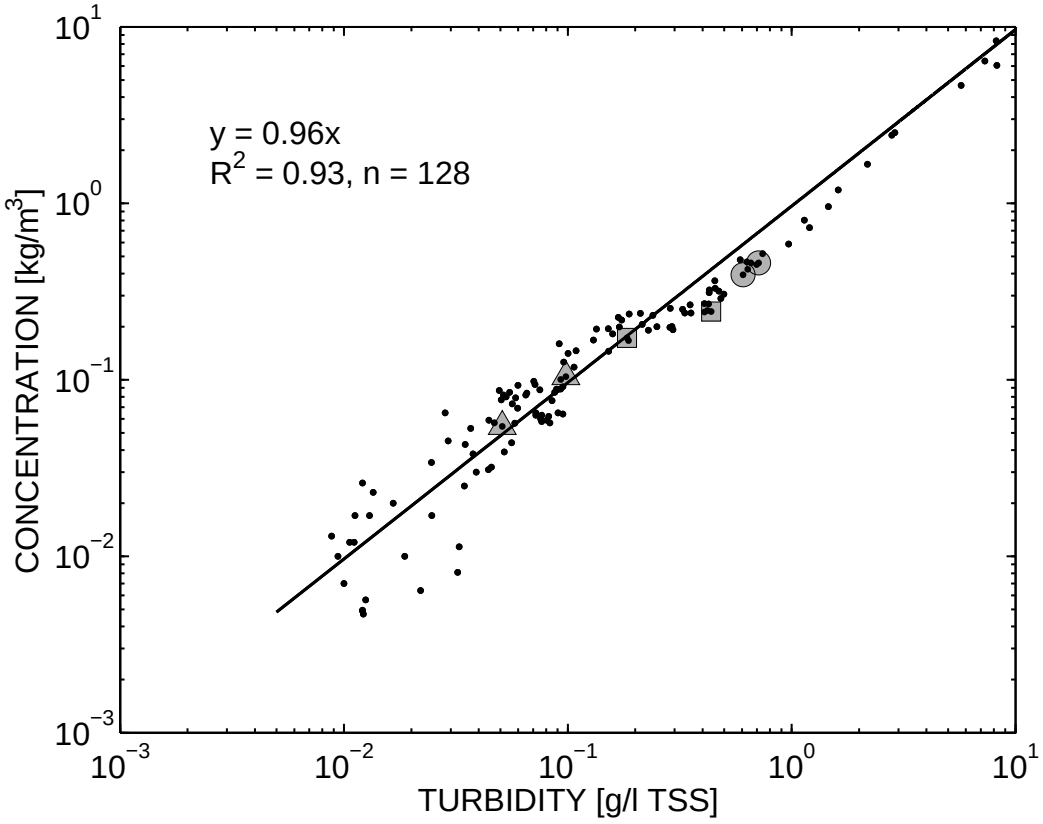

Fig. 4. Relationship between suspended sediment concentration measured in water samples and optical turbidity at Romans-sur-Isère. Units of turbidity for this graph are g/l Total Suspended Solids. The linear regression between concentration and turbidity was forced through the zero crossing of both variables. The number of data points and the coefficient of determination, R^2 are given. The water samples that had the unimodal, bimodal and trimodal primary particle size distributions shown in Figure 2 are plotted as circles, squares and triangles, respectively.

Author-produced version of the article published in Continental Shelf Research (2012), vol.46, p. 50-63
The original publication is available at http://www.sciencedirect.com/ doi : 10.1016/j.csr.2011.10.013

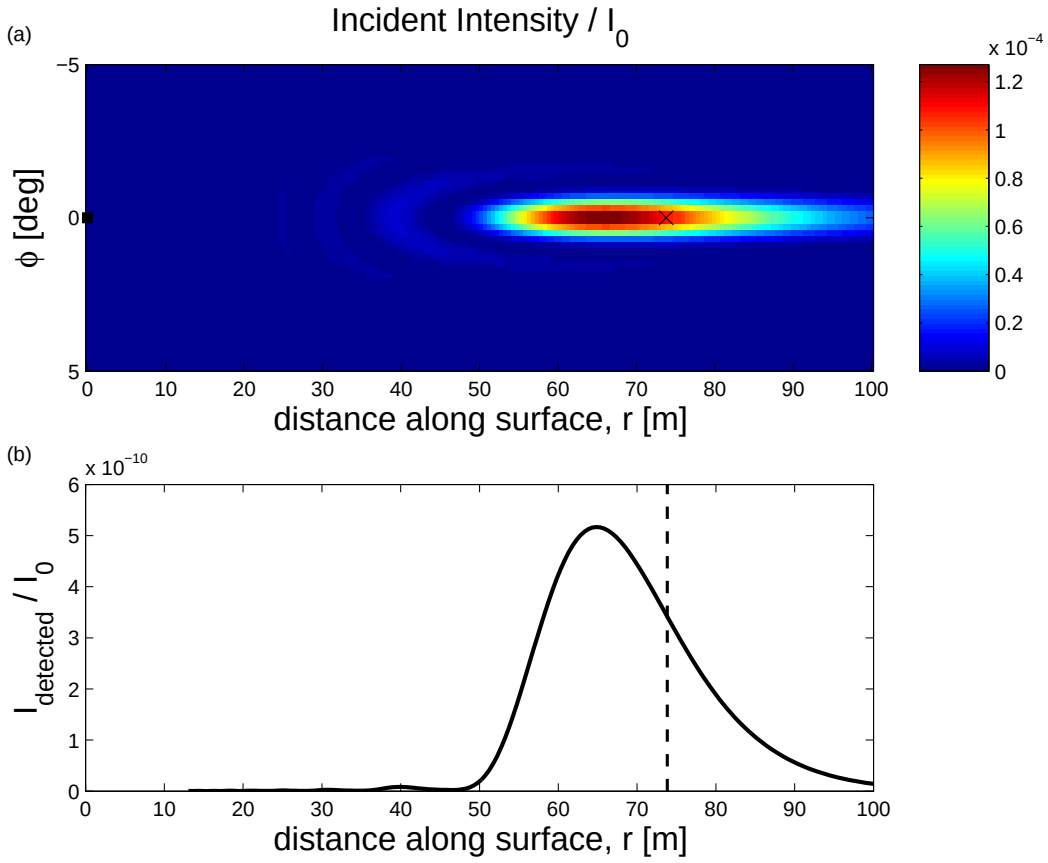

Fig. 5. [(a)] The theoretical intensity that is incident on the air-water interface for the 300 kHz H-ADCP at Romans-sur-Isère normalized by I_0. [(b)] The theoretical intensity detected by the 300 kHz H-ADCP for scattering from the air-water interface, normalized by I_0. The point of interception of the axis of the transducer with the surface is shown as a black x in subplot (a) and as a dashed-dotted line in subplot (b).

Author-produced version of the article published in Continental Shelf Research (2012), vol.46, p. 50-63
The original publication is available at http://www.sciencedirect.com/ doi : 10.1016/j.csr.2011.10.013

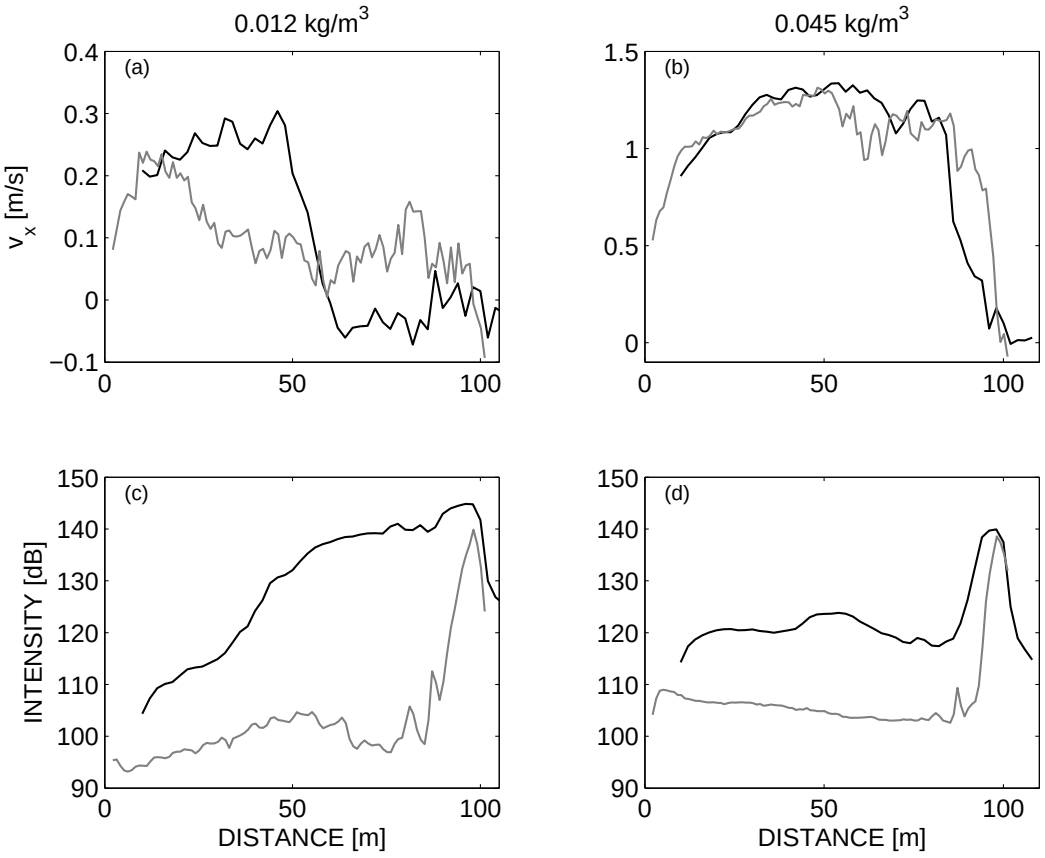

Fig. 6. Average streamwise velocity, v_x, measured by the 300 kHz (black line) and 600 kHz (gray line) H-ADCPs (a) November 25 2009 between 18:15 and 18:30 (UTC+1) and (b) May 4 2010 between 23:15 and 23:30 (UTC+1); [(c,d)] the corresponding range-corrected intensities measured by the central beam of each H-ADCP. Concentrations from the optical turbidity meter were 0.012 kg/m^3 November 25 and 0.045 kg/m^3 May 4 and the water levels were 0.09 m and 0.20 m, respectively. The distance from the right bank is plotted on the x axis.

Author-produced version of the article published in Continental Shelf Research (2012), vol.46, p. 50-63
The original publication is available at http://www.sciencedirect.com/ doi : 10.1016/j.csr.2011.10.013

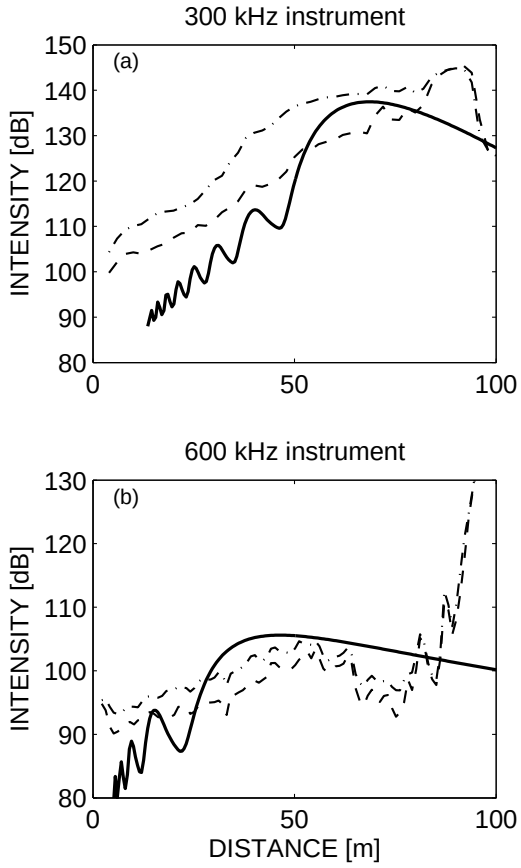

Fig. 7. Theoretical profiles of the range-corrected intensity for scattering from the air-water interface in the far field of the transducers (solid line) compared to measurements (dashed and dashed-dotted lines) with (a) the 300 kHz and (b) the 600 kHz H-ADCPs. Data are averaged over 15 minutes and the same time periods are used for both instruments. The water level for the data depicted as dashed-dotted lines was 0.09 m on the staff gauge, while that for the data depicted as dashed lines was 0.21 m.

Author-produced version of the article published in Continental Shelf Research (2012), vol.46, p. 50-63
The original publication is available at http://www.sciencedirect.com/ doi : 10.1016/j.csr.2011.10.013

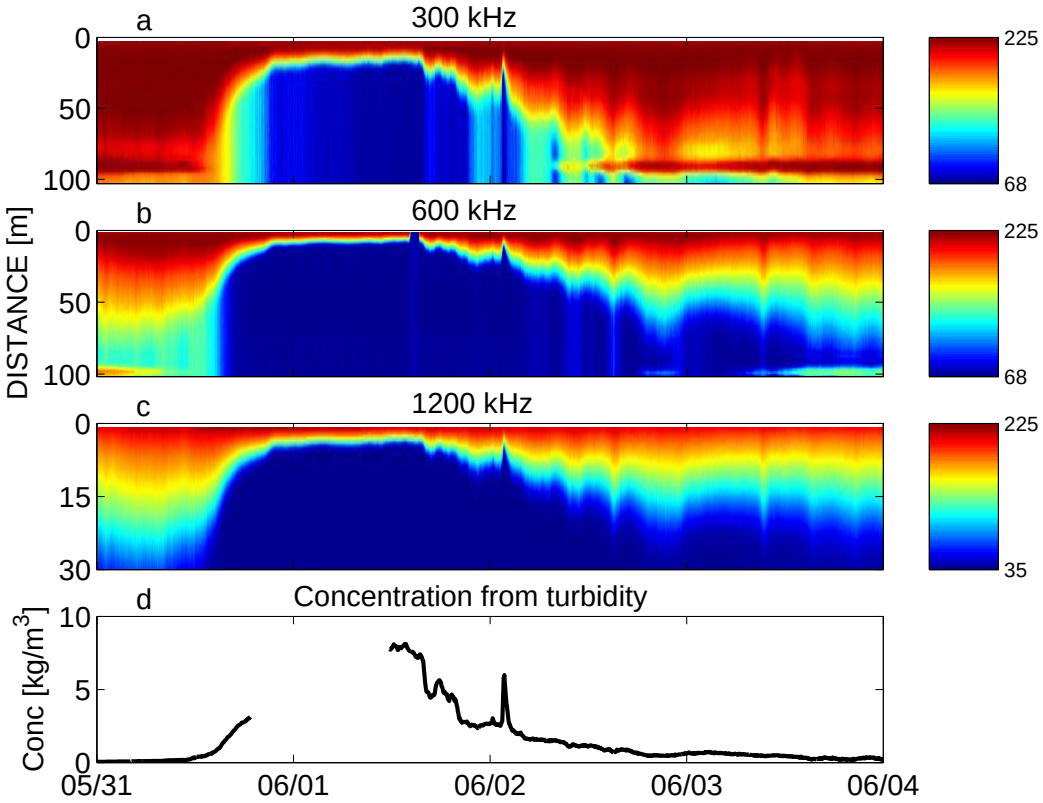

Fig. 8. Intensity data collected during and after the flood which occurred between May 31 2010 and June 3 2010 with: (a) beam 3 of the 300 kHz instrument, (b) beam 3 of the 600 kHz instrument and (c) beam 1 of the 1200 kHz instrument. The shading scale is logarithmic and covers the range of sensitivity of each instrument. Subplot (d) is the concentration time series from the optical turbidity data.

Author-produced version of the article published in Continental Shelf Research (2012), vol.46, p. 50-63
The original publication is available at http://www.sciencedirect.com/ doi : 10.1016/j.csr.2011.10.013

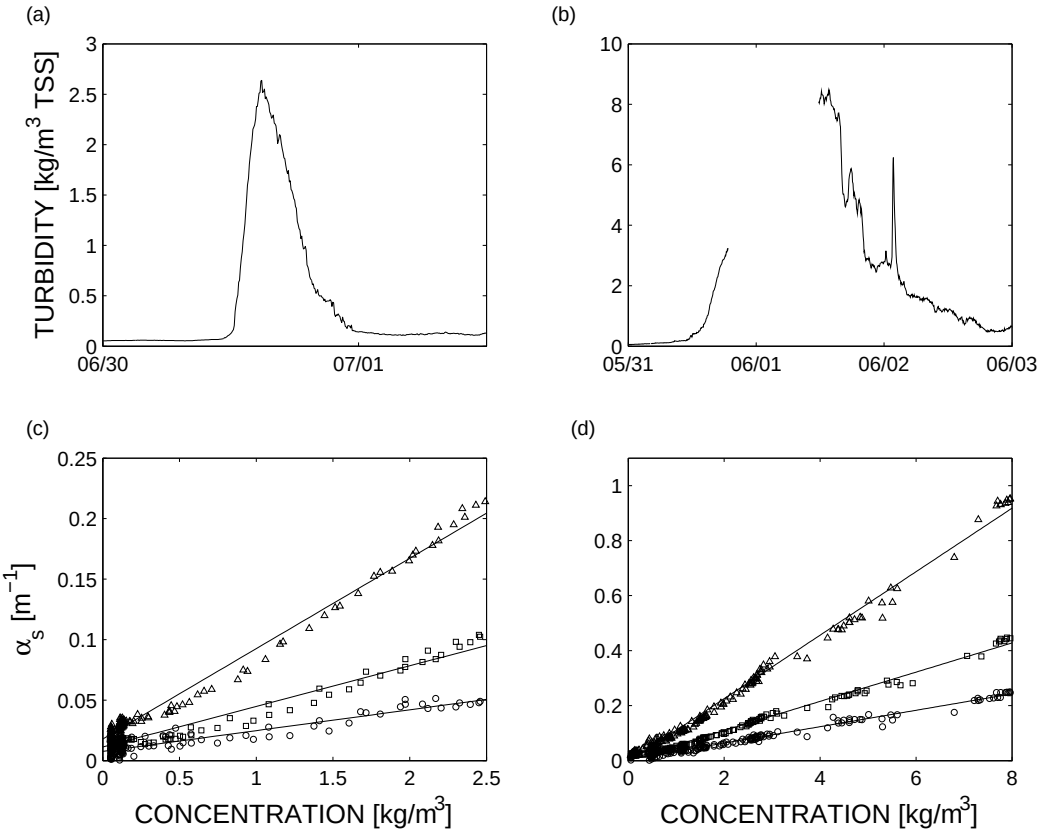

Fig. 9. Turbidity time series for the attenuation events of (a) June 30 2010 and (b) May 31 - June 3 2010. Relationship between particle concentration and sediment attenuation for the 300 kHz (circles), 600 kHz (squares), and 1200 kHz (triangles) H-ADCPs for (c) the June 30 event and (d) the May 31 - June 3 event. Concentrations are computed as 0.96 × turbidity and the least-squares linear fits to the data are shown.

Author-produced version of the article published in Continental Shelf Research (2012), vol.46, p. 50-63
The original publication is available at http://www.sciencedirect.com/ doi : 10.1016/j.csr.2011.10.013

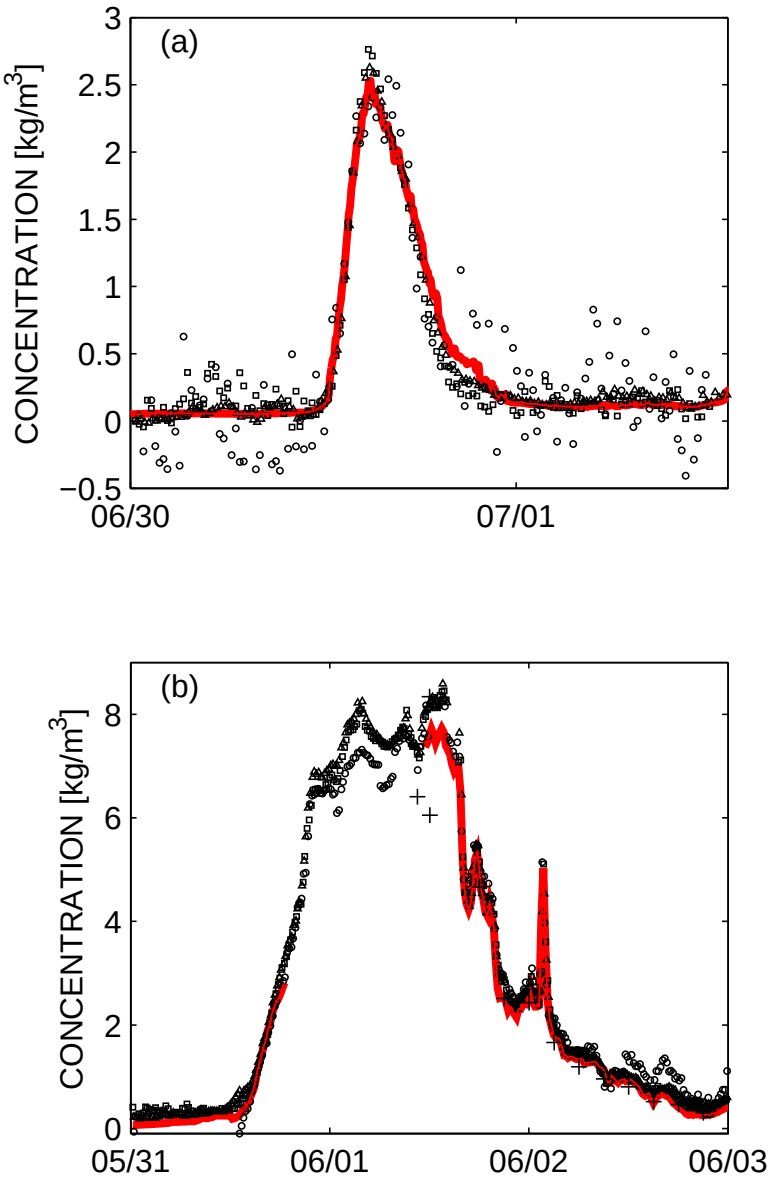

Fig. 10. A comparison between concentration values measured in water samples (plus signs) and obtained with the optical turbidity data (solid red or gray line) and the sediment attenuation data from the 300 kHz (circles), 600 kHz (squares), and 1200 kHz (triangles) H-ADCPs for (a) the June 30 event and (b) the spring flood.